PERGAMON

Renewable Energy 24 (2001) 1–18

RENEWABLE ENERGY

www.elsevier.nl/locate/renene

A vortex model for Darrieus turbine using finite element techniques

Fernando L. Ponta [a,*], Pablo M. Jacovkis [b]

[a] *Grupo ISEP, Departamento de Electrotecnia, Facultad de Ingeniería, Universidad de Buenos Aires, Paseo Colón 850 (1063) Buenos Aires, Argentina*

[b] *Departamento de Computación and Instituto de Cálculo, Facultad de Ciencias Exactas y Naturales, Universidad de Buenos Aires, Ciudad Universitaria (1428) Buenos Aires, Argentina*

Received 23 August 2000; accepted 4 October 2000

Abstract

Since 1970 several aerodynamic prediction models have been formulated for the Darrieus turbine. We can identify two families of models: stream-tube and vortex. The former needs much less computation time but the latter is more accurate. The purpose of this paper is to show a new option for modelling the aerodynamic behaviour of Darrieus turbines. The idea is to combine a classic free vortex model with a finite element analysis of the flow in the surroundings of the blades. This avoids some of the remaining deficiencies in classic vortex models. The agreement between analysis and experiment when predicting instantaneous blade forces and near wake flow behind the rotor is better than the one obtained in previous models.
© 2001 Elsevier Science Ltd. All rights reserved.

Keywords: Darrieus turbine; Free vortex model; Finite element; Vertical axis wind turbine; Numerical modelling

1. Introduction

The Darrieus Turbine is a kind of power machine used originally in wind–power applications and recently applied to hydropower generation. These turbines have several advantages, but the prediction of their behaviour is more complex than the prediction of the horizontal-axis turbines.

* Corresponding author. Tel.: +54-11-4343-0891 Int: 363; fax: +54-11-4343-0891 Int: 365.
E-mail addresses: fponta@fi.uba.ar (F.L. Ponta), jacovkis@dc.uba.ar (P.M. Jacovkis).

0960-1481/01/$ - see front matter © 2001 Elsevier Science Ltd. All rights reserved.
PII: S0960-1481(00)00190-7

Since 1970 several aerodynamic prediction models have been formulated for Darrieus machines. Modelling of these turbines follows two different schools: the stream-tube modelling approach, that is based upon equating the forces on the rotor blade to the change in streamwise momentum through the rotor, and the vortex modelling approach, that is based upon vortex representations of the blades and their wakes. The stream-tube approach needs much less computation time but the vortex approach is more accurate.

Stream-tube models have evolved with time and we can distinguish several categories. The first of them is the *Single Stream-Tube Model* proposed by Templin [1]. It uses a single tube that covers the entire span of the rotor. The latter's interference is represented by an actuator disk. As the entire rotor is represented by only one tube with one actuator disk, this model predicts a uniform flow for the entire cross section and can not take into account variations of the flow parameters between the upwind and downwind halves of the rotor. To improve the predictive capacities Strickland [2] proposed the *Multiple Stream-Tube Model*, which uses an array of adjacent tubes to cover the rotor's span. It permits to know the flow variations over the cross section. A more sophisticated approach called *Double-Multiple Stream-Tube Model* was proposed by Paraschivoiu [3]. As it uses two actuator disks placed in tandem into each tube of the multiple array, it can also predict differences between the upwind and downwind halves. Advanced versions of Paraschivoiu's model incorporate dynamic stall models. Stream-tube models (specially Paraschivoiu's) can predict effectively the general performance of the rotor (power coefficient vs. TSR, power output vs. wind speed, etc.) and their relatively low computational cost makes them a useful practical tool for design. On the other hand, they exhibit differences predicting the instantaneous forces on the blades. To calculate accurately these forces we have to use a vortex model; the following sections aboard this subject.

2. Free vortex model

A very useful method developed for the Darrieus turbine analysis is the free vortex model. It is based upon the replacement of the airfoil blade by a bound vortex filament called a *lifting line* that changes its strength as a function of azimutal position. The use of a single line vortex to represent the airfoil is a simplification over the two-dimensional vortex model of Fanucci and Walters [4] that uses three to eight bound vortices positioned along the camber line. A single bound vortex represents the flow field adequately at distances greater than about one chord length from the airfoil ([5]). Fig. 1 shows the bounded and the shed filaments for a blade element. Fig. 2 shows the trajectory of a vortex wake.

Because of the bound vortex variation, spanwise vortices were shed and their strengths are equal to the change in the bound vortex strength. Thus, the wake is modelled by a discrete set of free vortex filaments shed from the each blade end in such a way so as to satisfy Kelvin's theorem in a discrete way:

$$\Gamma_{sN-1}=\Gamma_{bN-1}-\Gamma_{bN}, \tag{1}$$

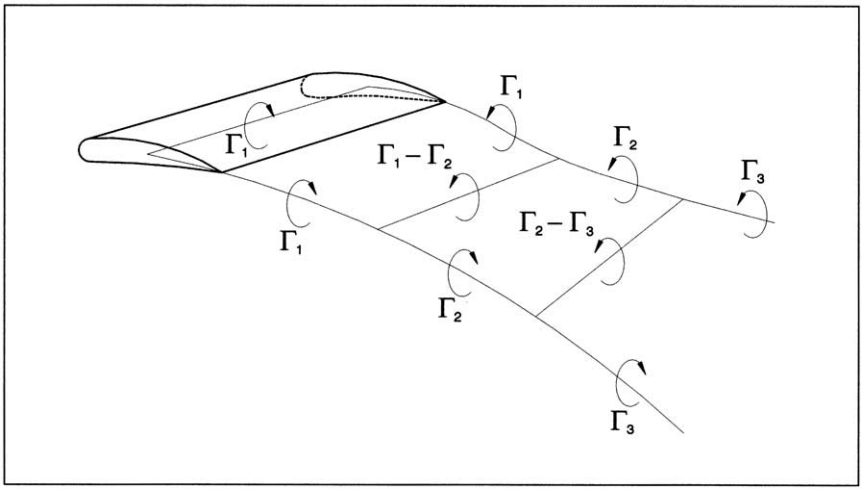

Fig. 1. Vortex structure for a blade element.

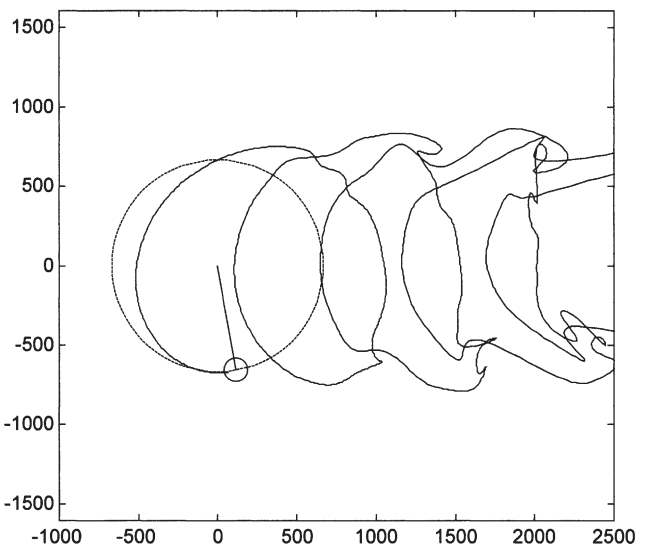

Fig. 2. An example of a shed vortex wake calculated by the FEVDTM model.

where Γ_{sN-1} is the strength of the vortex shed at $N-1$ iteration, Γ_{bN} is the bound vortex strength at N iteration and Γ_{bN-1} is the bound vortex strength at $N-1$ iteration.

Shed vortex filaments are convected downstream at the local flow velocity. The flow velocity at any point is determined by the sum of the undisturbed free stream velocity and the velocity induced by the entire vortex filaments in the flow field. The velocity induced at a point by a single vortex filament is calculated from the

Biot–Savart law. In two-dimensional analysis, corresponding to straight bladed rotors, infinite length rectilinear filaments perpendicular to flow plane can be used. Then, the induced velocity at a point p is given by:

$$\underline{v}_p=(\underline{r}\wedge\hat{k})\frac{\Gamma}{2\pi h}, \tag{2}$$

where h is the perpendicular distance from the vortex filament to p, $\underline{r}$ is the unit vector in the direction from the vortex filament to p and $\hat{k}$ is the unit vector in the direction perpendicular to flow plane.

In order to allow closure of the proposed vortex model, a relationship between the bound vortex strength and the local flow velocity at the blade must be obtained. Up to the present, several techniques were developed to achieve this. One of the most successful, proposed by Strickland et al. [6], equates the lift per unit span on the blade with the one formulated in terms of the airfoil section lift coefficient. It yields the required relationship between the bound vortex strength Γ_b and the local relative velocity in the plane of the airfoil section W_R.

$$\Gamma_b=\frac{1}{2}c_l c W_R, \tag{3}$$

where c_l is the airfoil section lift coefficient and c is the blade chord.

It should be noted that the effects of aerodynamic stall are automatically included into Eq. (3) through the section lift coefficient.

A curve-bladed rotor requires a three-dimensional analysis where its blades are divided into a number of segments along their span. A rectilinear bound vortex filament replaces each blade element. Spanwise vortices are shed from each of them in a way that satisfies Kelvin's theorem. It can be assumed that the elemental vortex filament remains straight with its ends being convected at their respective local fluid velocities. Therefore, they may stretch, translate and rotate as a function of time. At the end of each blade element, a trailing vortex is shed as a consequence of the Helmholtz theorem of vorticity (conservation of Γ along a vortex tube). It results in shedding a quadrilateral mesh vortex system with concentrated vortices of equal strength along each side. Spanwise and trailing vortices which are shed during any given time period can be related to the change in bound vorticity with respect to time and position along the blade. The velocity induced at any point in three dimensions by each finite length vortex filament is calculated from the Biot–Savart law using an expression slightly more complex than Eq. (2). Strickland's model can treat both straight and curve-bladed rotors.

2.1. Considerations

The free vortex model has several advantages over the previous methods. There are, however, shortcomings of this approach:

1. All of the aerodynamic models described above require airfoil coefficients taken

from static test data for their use. Since Darrieus rotor blades rotating at angular velocity ω experience significant cyclic variations in relative velocity and angle of attack, the use of quasi-steady aerodynamics for the determination of forces has been questioned. There is another version of free vortex model developed by Wilson et al. [7] which, instead of calculating the aerodynamic loads from the airfoil coefficient data, uses an analytical method to perform this. It employs the circle theorem to map the airfoil into a circle plane where the Kutta condition is satisfied and the strength of the vortices are determined. The force on the airfoil is determined by two methods, integration of the pressure over the airfoil and impulse of the wake vortices. This solution avoids the quasi-steady approach; however, it introduces another two disadvantages: first, it does not cover stall phenomena; second, it is based upon the complex potential theory that requires the irrotational flow condition and it is not real because, still under the assumption of non-viscous flow, there exists a rotational effect induced by turbine rotation that potential flow theory can not manage.

2. Circulation about a pitching airfoil operating over a curvilinear path differs from those found on non-pitching, non-rotating sections. Surface pressure distribution differs too, and it would alter the boundary layer structure and therefore the section characteristics.
3. Another unsteady effect is due to fluid inertia. There are non-circulatory forces proportional to airspeed changes and angular velocity. These fall into the category of apparent mass effects.

Wilson and Strickland included adjustment terms in their models to compensate for the effects of pitching circulation and apparent mass.

3. Free vortex model combined with finite element analysis (FEVDTM)

The purpose of the present paper is to show a new option for modelling the aerodynamic behaviour of Darrieus turbines avoiding some of the remaining deficiencies in classic free vortex models. The idea is to combine a free vortex model with a finite element analysis of the flow in the surroundings of the blades. The free vortex scheme acts as a macro-model whose results are used as a boundary condition on the boundary of the finite element analysis area Ω, which acts as a micro-model (see Fig. 3). The bound vortex strength is determined by integration of the flow velocity field obtained from the finite element analysis. This sequence defines an iterative scheme; after it converges we can calculate the surface pressure distribution over the airfoil integrating the momentum equation. From this knowledge of pressure and velocity distributions, we can input a boundary layer model to calculate the viscous shear stress over the airfoil surface. The aerodynamic forces on the blade are determined by integration of these pressure and shear stress distributions. A pseudo code diagram of the FEVDTM program is shown in Fig. 4.

This model has the following advantages:

1. It does not use airfoil coefficient data, thus avoiding the quasi-steady approach

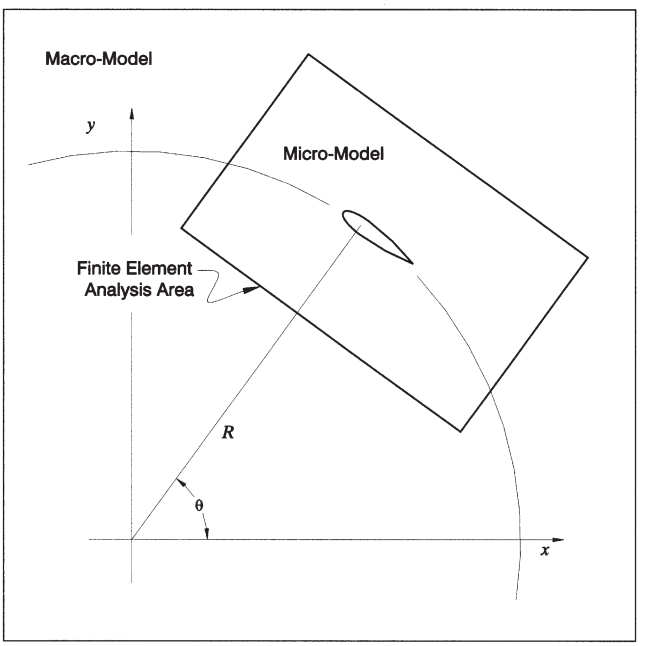

Fig. 3. Micro-model diagram and finite element analysis area.

problem; moreover, it does not suffer from the irrotational flow condition of potential analysis because, as we shall see later, we can solve our finite element analysis considering the rotational effect induced by turbine rotation.

2. Every point of the micro-model boundary has its corresponding velocity input, including the rotational velocity components. Therefore, the finite element analysis is made under curvilinear flow boundary conditions; thus, pitching circulation effect is naturally included.
3. Apparent mass effects can be calculated exactly because they are included in the momentum equation.

It should be noted that this model does not include the stall phenomena. When stall occurs, the boundary layer separates from the solid contour of the airfoil and a turbulent wake appears. Up to the present, mathematical modelling of turbulent wakes is extremely complex (and expensive in terms of computer time). Therefore, we can apply the new model before stall appearance, switching to a classical free vortex model using airfoil coefficient data when stall condition is detected.

4. The finite element analysis for the micro-model

As we stated above, we shall consider the viscous effects restricted to the boundary layer and the external flow as non-viscous. There are three options to perform the

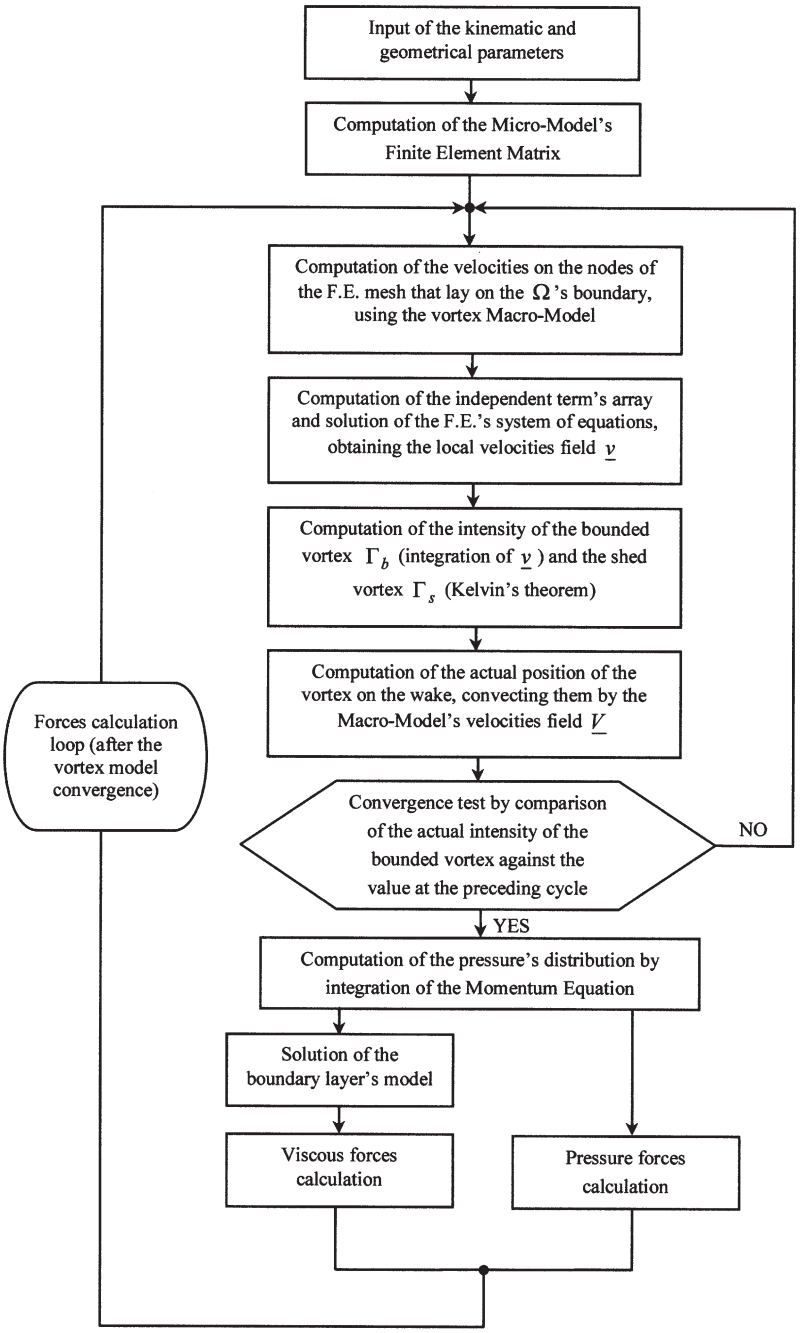

Fig. 4. Pseudo-code diagram of the FEVDTM program.

micro-model analysis; two of them are quite well-known and the other is a new attempt that will be treated in detail afterwards. These options are:

1. Potential Flow Equation — It has the advantage that it is economic to compute because: a) there is just one variable per node to solve, b) incompressibility condition is automatically implicit in the equation formulation and c) the equation is linear; thus, it means a direct solution without iterative schemes. On the other hand, due to the irrotational flow condition of potential analysis, the problem of the exclusion of the rotational effect induced by turbine rotation still remains.
2. Euler Equation — The obvious option for our problem is to solve the momentum equation using Petrov–Galerkin techniques; for example, imposing incompressibility by penalty, Lagrangian multipliers or augmented Lagrangian methods. This option is quite valid; however, it implies an iterative resolution because of the nonlinearity introduced by the convective term in the momentum equation. Moreover, due to the non-steadiness of this phenomenon, we have to use some method to treat the time-dependent term (Crank–Nicholson, for example) and it introduces an additional complication to the scheme. It means that we have to solve an iterative process for the micro-model inside the macro-model iterative process. Considering that the free-vortex approach is largely voracious on the computational resources concerned, this inclusion of a loop within a loop can become too time-consuming for a practical solution.
3. Constant-Curl Laplacian Equation — This is a new attempt that owns the simplicity and linearity of a potential analysis but includes the rotational effect induced by turbine rotation taking advantage of the fact that this rotation is constant. The idea is based upon a kinematic scheme that states the nullity of the velocity Laplacian imposing simultaneously the conditions of incompressibility and constant curl for the velocity field.

A well-known vector relation states

$$\nabla^2 \underline{v} = \underline{\nabla} \cdot \underline{\nabla}\, \underline{v} = \underline{\nabla}(\underline{\nabla} \cdot \underline{v}) - \underline{\nabla} \wedge (\underline{\nabla} \wedge \underline{v}) \tag{4}$$

where $\underline{v}$ is the velocity vector in a moving reference frame fixed to the blade. By the incompressibility condition $(\underline{\nabla} \cdot \underline{v})=0$, the first term of the third member of Eq. (4) vanishes. Thus, if the curl of the velocity field $rot\,\underline{v}=(\underline{\nabla} \wedge \underline{v})$ is constant, it yields:

$$\nabla^2 \underline{v} = \underline{\nabla} \cdot \underline{\nabla}\, \underline{v} = 0 \tag{5}$$

It can be proved for the case of Darrieus turbine (for a brief summary of the proof see Appendix A) that the curl of the velocity field external to the boundary layer inside the micro-model control volume is:

$$rot\ \underline{v} = -2\omega \hat{k} \tag{6}$$

where ω is the angular speed of the turbine (assumed constant) and $\hat{k}$ is the unit vector normal to the frame.

Thus, the curl is constant and Eq. (5) holds. A finite element routine that solves this equation with the constraints of incompressibility ($\underline{\nabla}\cdot\underline{v}$)=0 and constant-curl $\underline{\nabla}\wedge(\underline{\nabla}\wedge\underline{v})$=0 was implemented [8].

We use 9-nodes isoparametric elements interpolating velocities and imposing the constant-curl condition by a modified penalty method and incompressibility by a classical one. The 9-nodes isoparametric element has a great power of convergence due to its biquadratic interpolation functions (including a bubble function on the 9*n*th node); it allows the use of coarser meshes than, for instance, triangular element's. And, as the geometrical coordinates are mapped by the same functions, these elements could have curvilinear sides, so they can reproduce the airfoil's curvilinear shapes more accurately than classical elements because of the quasi elimination of the so called *skin error*.

On the other hand, the constant-curl Laplacian equation presents a very interesting numerical advantage against potential-flow: we are interpolating directly the velocities field (instead of a potential whose gradient gives us the velocity). This fact implies that the exponent of the convergence index is greater than the potential-flow's, increasing the convergence rate (allowing the use of coarser meshes) and making this option computationally cheaper. Fig. 5 shows the finite element mesh used for calculation of a NACA 0012 bladed rotor and Fig. 6 shows a detailed view.

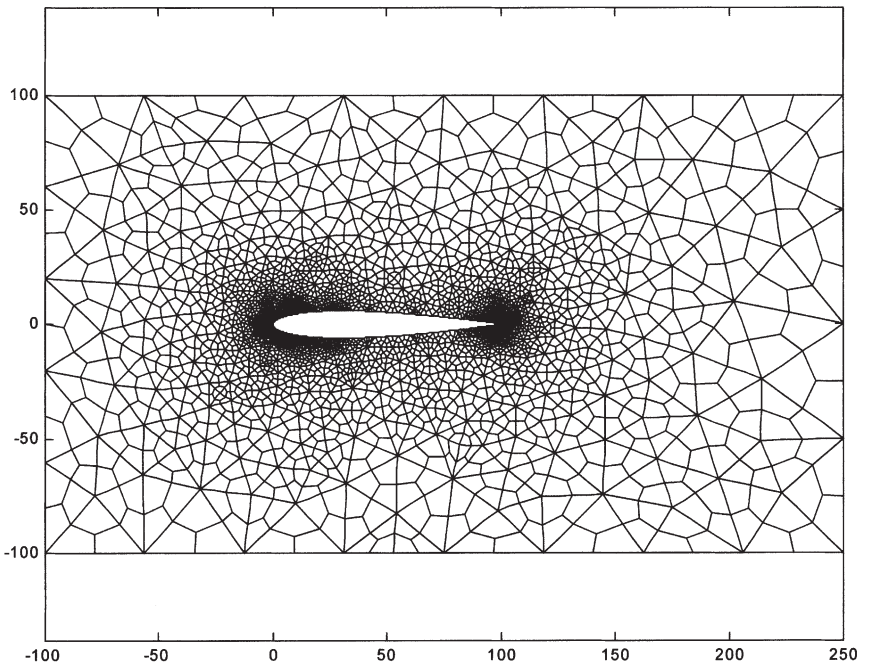

Fig. 5. Finite element mesh used for calculation of a NACA 0012 blade.

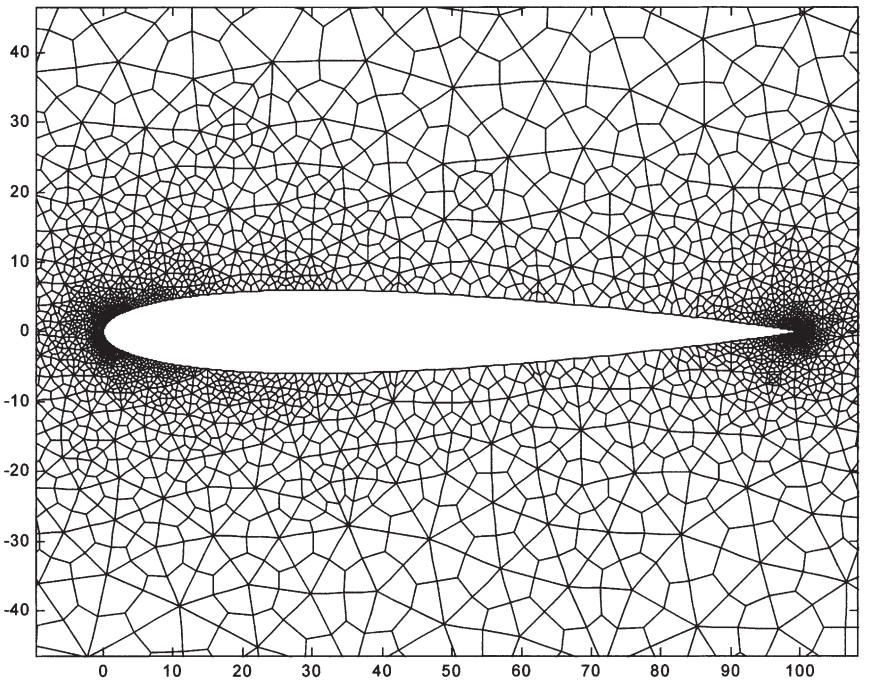

Fig. 6. Detailed view of the finite element mesh for the NACA 0012 blade.

5. Aerodynamic forces calculation

Once the iterative micro-macro scheme has converged we proceed to the calculation of the aerodynamic forces over the blades.

Pressure distribution is calculated by integration of momentum equation. For the micro-model's moving reference frame, momentum equation states:

$$\frac{\partial \underline{v}}{\partial t}+\frac{1}{2}\underline{\nabla}|\underline{v}|^2+\frac{1}{\rho}\underline{\nabla}p-\omega^2 R\hat{j}-\frac{\omega^2}{2}\underline{\nabla}|\underline{z}|^2=0 \tag{7}$$

where p is the thermodynamic pressure, R is the turbine radius, ρ is the fluid density and t is the time. The position vector with respect to the moving micro-model's system of coordinates is $\underline{z}$ (see Fig. 7) with components z_1, z_2 and z_3; the respective unit vectors are $\hat{i},\hat{j}$ and $\hat{k}$.

Integrating over a curvilinear path from the leading edge to any generic point P on the contour of the airfoil and doing some algebra, we arrive at the following expression:

$$p_P=p_0+\frac{\rho}{2}(v_0^2-v_P^2)+\frac{\rho\omega^2}{2}(z_P^2-z_0^2)+\rho\omega^2 R(z_{2P}-z_{20})-\rho\int_0^{l_P}\frac{\partial \underline{v}}{\partial t}\cdot\hat{t}dl \tag{8}$$

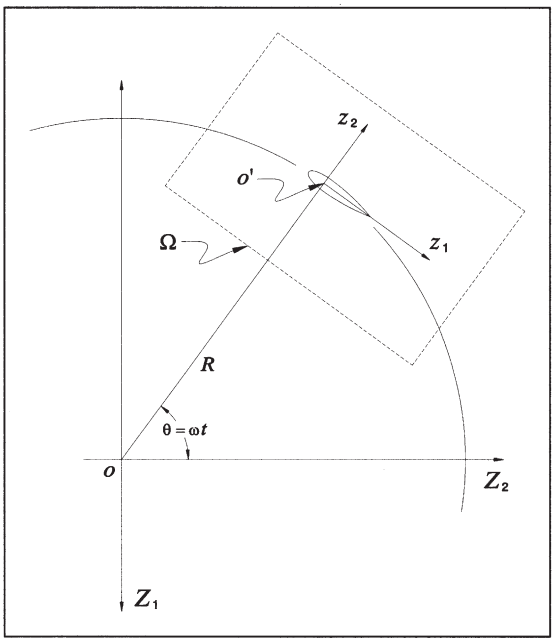

Fig. 7. Micro-model's system of coordinates.

where p_P is the pressure at a point P, l is the curvilinear coordinate, $\hat{t}$ is the unit vector tangent to the airfoil contour, z is the modulus of vector $\underline{z}$ and v is the modulus of vector $\underline{v}$ (v_0 and z_0 are the values at the leading edge, and v_P and z_P the values at a point P). z_{2P} and z_{20} are the values of z_2 (the second coordinate of the micro-model's system) at a point P and at the leading edge respectively.

The time derivative could be estimated using data from two consecutive instants. The pressure at the leading edge p_0 has no influence over the resulting force because is equivalent to a uniform pressure acting on the total contour of the airfoil; thus, we shall assign it a zero value.

To calculate viscous forces we shall use the Von Karman integral momentum equation for boundary layer:

$$\delta\frac{dp}{dl}+\tau_w=U\frac{d}{dl}\int_0^{\delta}\rho u dy-\frac{d}{dl}\int_0^{\delta}\rho u^2 dy \tag{9}$$

where δ is the boundary layer thickness, U is the velocity on the boundary layer external border, u is the velocity inside the boundary layer, y is the coordinate perpendicular to the airfoil contour and τ_w is the shear stress on the airfoil contour.

To implement the Von Karman model we have to assume a velocity profile inside the boundary layer and a relationship between shear stress τ_w and flow parameters (U,δ). For laminar boundary layers it is usual to assume a quadratic velocity profile

and to employ the Newton's viscosity law to relate the stresses. Replacing Eq. (9) and doing some algebra, it yields:

$$\frac{d\delta}{dl}=\frac{15}{2U^2}\left(\frac{2U\eta}{\delta}+\delta\left(\frac{1}{\rho}\frac{dp}{dl}+\frac{6}{15}U\frac{dU}{dl}\right)\right) \tag{10}$$

$$\tau_w=\frac{2\eta\rho U}{\delta}, \tag{11}$$

where η is the kinematic viscosity. Eq. (10) was solved using a fourth order Runge–Kutta algorithm beginning from the stagnation-point and following separately the upper and lower sides of the airfoil contour towards the trailing edge. Afterwards, we use Eq. (11) to obtain the stresses.

Pressures and shear stresses were integrated along the airfoil contour to obtain the total aerodynamic forces actuating on the blade.

6. Validation of the FEVDTM model

To test the behaviour of the FEVDTM model we simulated a case studied by Strickland and included by Klimas in [9]. It was an experimental test over a NACA 0012 two-bladed Darrieus rotor where normal and tangential forces acting on the blade were measured as a function of time using a strain gages arrangement. The test was made at a tip to wind speed ratio of 5, a blade Reynolds' number of 40,000 and a 0.15 chord-radius ratio. Fig. 8 shows the non-dimensional normal force against the azimutal angle after the third revolution comparing experimental data, the Strickland's model V–DART and FEVDTM predictions. Fig. 9 shows the non-dimensional tangential force case.

Strickland et al. [6] also studied the wake's conformation by dye injection through the trailing edge of one of the rotor blade airfoils. This streak line is indicative of the vortex sheet produced by the airfoil or it can be thought of as a line made up of shed vortex centres. A NACA 0012 straight bladed rotor with 1, 2 and 3 blades was tested. Figs. 10–12 show respectively for these three cases, the FEVDTM prediction superimposed over the experimental visualisation.

7. Conclusions

The results shown in Figs. 8 and 9 clearly confirm the advantages of FEVDTM compared against the earlier models in predicting instantaneous blade forces as well as wake constitution. Figs. 10–12 show comparisons for one-bladed, two-bladed and three-bladed rotors respectively. That represents a range of significant cases for which experimental wake-structure data exist.

The idea of splitting the analysis into two separate regions (micro and macro models) allows us to improve the accuracy of the single lifting line approach. That is because we use the results of the vortex macro-model at the border of Ω, i.e., at

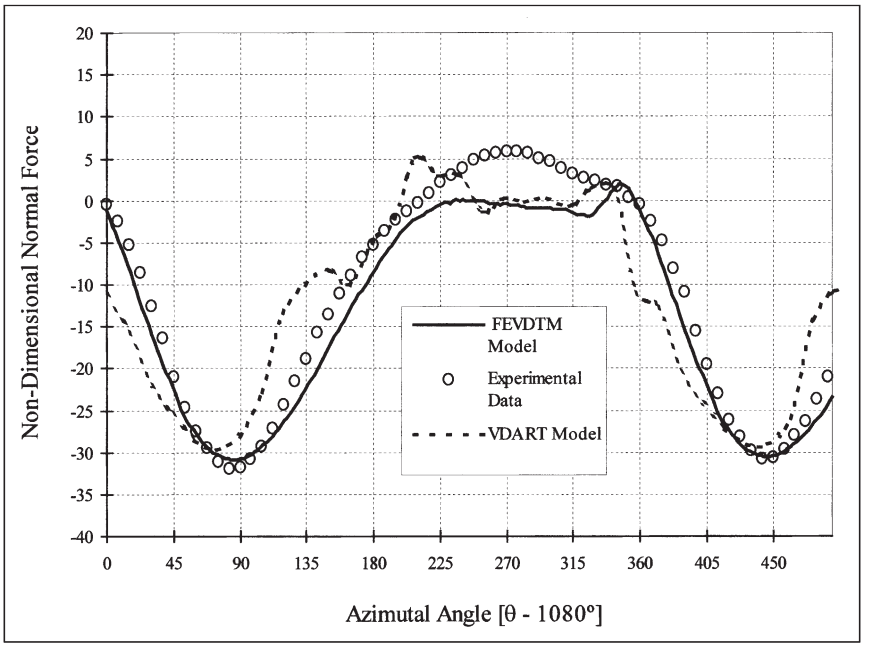

Fig. 8. Non-dimensional normal force against the azimutal angle after the third revolution. Comparison of experimental data, V–DART [8] and FEVDTM predictions.

a distance at least one and half of chord length from the airfoil where the velocities field induced by a single lifting line is acceptable.

The Constant-Curl Laplacian Equation has the advantage that we do not need to calculate separately the rotational effects; they are included automatically in the velocities used as boundary conditions for the micro-model calculation.

We remark that this model does not cover stall phenomena, but it provides instantaneous data of the flow at the border of the boundary layer that can be used to detect the stall appearance. So, FEVDTM is a full theoretical tool that could be used as the basis of a future more sophisticated model that includes theoretical stall simulation.

Acknowledgements

The authors gratefully acknowledge the financial support of University of Buenos Aires through grants AI–09 and TW–91.

Appendix A

To prove the constant-curl condition we shall start analysing the velocities on the external boundary of Ω, writing them with respect to a reference frame fixed to the

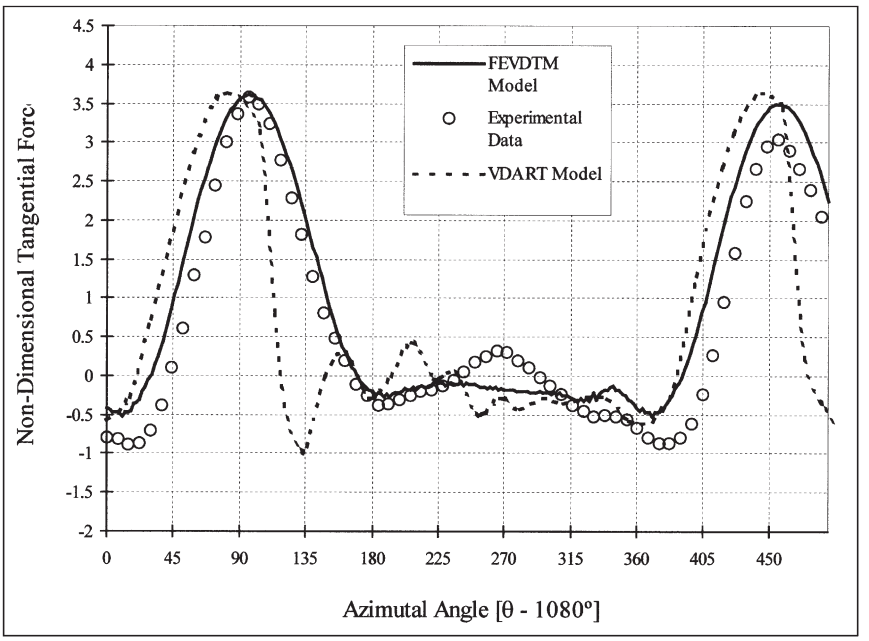

Fig. 9. Non-dimensional tangential force against the azimutal angle.

moving airfoil. Considering that that boundary is sufficiently far from the airfoil, we can neglect the latter's influence, so that those velocities are given by the macro-model calculation and their subsequent transformation into the moving reference frame. We shall start with the geometrical-coordinate's transformation. From Fig. 7:

$$\underline{Z}(t)=\underline{\underline{Q}}(t)\cdot\underline{z}(t)+\underline{Z}_{0'}(t) \tag{A1}$$

where $\underline{Z}(t)$ is the position vector with respect to the fixed frame, $\underline{\underline{Q}}(t)$ is the orthogonal matrix that performs the moving-to-fixed frames transformation, $\underline{Z}_{0'}(t)$ is the position vector of the origin of coordinates of the moving frame and $\underline{z}(t)$ is the position vector with respect to the moving frame.

Taking derivatives with respect of the time:

$$\dot{\underline{Z}}(t)=\underline{\underline{\Psi}}\cdot\underline{\underline{Q}}(t)\cdot\underline{z}(t)+\underline{\underline{Q}}(t)\cdot\dot{\underline{z}}(t)+\dot{\underline{Z}}_{0'}(t) \tag{A2}$$

where $\dot{\underline{Z}}_{0'}(t)=\underline{V}_{0'}(t)=\omega\hat{k}\wedge R\hat{j}$ is the velocity of the origin of coordinates of the moving frame, $\underline{\underline{\Psi}}$ is the skew-symmetric matrix that of the rotation speed of the moving frame so that $\dot{\underline{\underline{Q}}}(t)=\underline{\underline{\Psi}}\cdot\underline{\underline{Q}}(t)$, $\dot{\underline{z}}(t)=\underline{v}$ is the velocity of any point with respect to the moving frame and $\dot{\underline{Z}}(t)=\underline{V}$ is the velocity of any point with respect to the fixed frame (given by the macro-model).

After some algebraic manipulation we get:

$$\dot{\underline{z}}(t)=\underline{\underline{Q}}^{T}(t)\cdot(-\underline{\underline{\Psi}}\cdot\underline{\underline{Q}}(t)\cdot\underline{z}(t)+\dot{\underline{Z}}(t)-\dot{\underline{Z}}_{0'}(t)) \tag{A3}$$

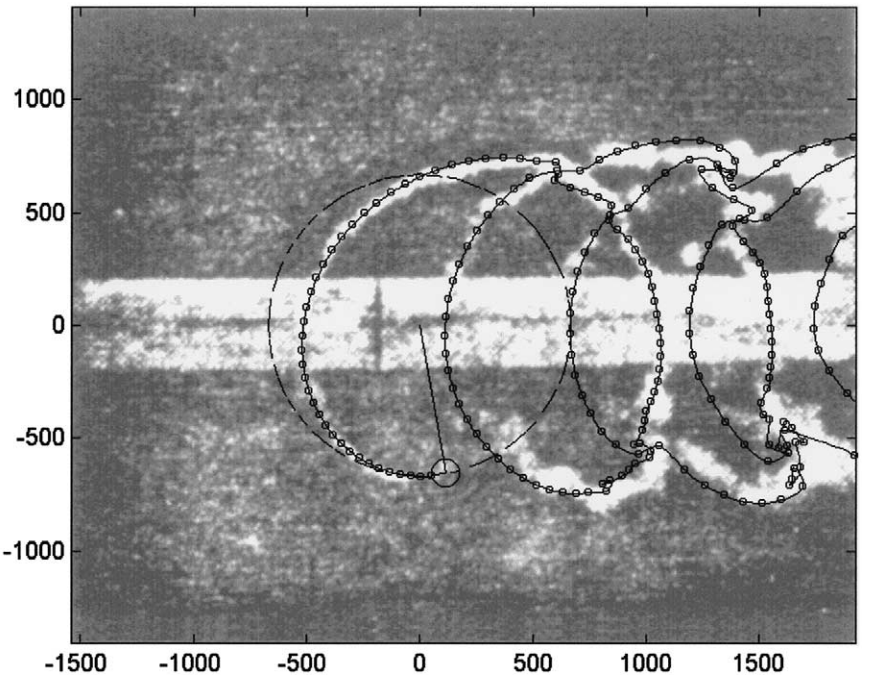

Fig. 10. Shed vortex centres path for a one-bladed rotor. Comparison of experimental visualisation [6] and FEVDTM prediction.

$$\underline{v}=\dot{\underline{z}}=[\underline{\underline{Q}}^T]\cdot\left(-\underbrace{\begin{bmatrix}0 & -\omega & 0\\ \omega & 0 & 0\\ 0 & 0 & 0\end{bmatrix}}_{\underline{\underline{\psi}}}\cdot\underbrace{\begin{bmatrix}\cos\omega t & -\mathrm{sen}\omega t & 0\\ \mathrm{sen}\omega t & \cos\omega t & 0\\ 0 & 0 & 1\end{bmatrix}}_{\underline{\underline{Q}}}\cdot\begin{bmatrix}z_1\\ z_2\\ z_3\end{bmatrix}+[\underline{V}]-[\underline{V}_{0'}]\right) \tag{A4}$$

$$\underline{v}=-\begin{bmatrix}\cos\omega t & \mathrm{sen}\omega t & 0\\ -\mathrm{sen}\omega t & \cos\omega t & 0\\ 0 & 0 & 1\end{bmatrix}\cdot\begin{bmatrix}-\omega z_1\mathrm{sen}\omega t-\omega z_2\cos\omega t\\ \omega z_1\cos\omega t-\omega z_2\mathrm{sen}\omega t\\ 0\end{bmatrix}+[\underline{\underline{Q}}^T]\cdot([\underline{V}]-[\underline{V}_{0'}]) \tag{A5}$$

$$\underline{v}=-\begin{bmatrix}-\omega z_2\\ \omega z_1\\ 0\end{bmatrix}+[\underline{\underline{Q}}^T]\cdot([\underline{V}]-[\underline{V}_{0'}]) \tag{A6}$$

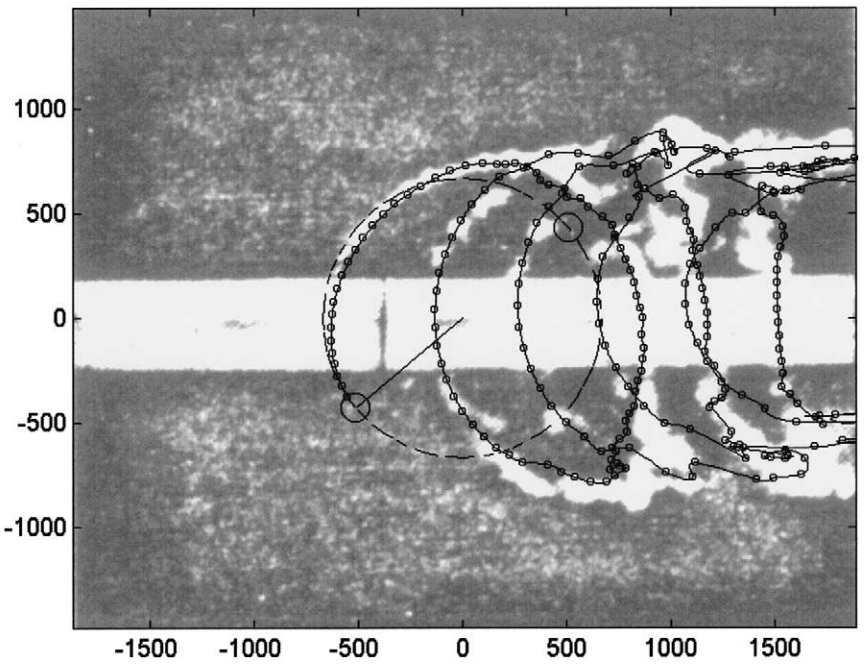

Fig. 11. Shed vortex centres path for a two-bladed rotor. Comparison of experimental visualisation [6] and FEVDTM prediction.

Then, the curl of $\underline{v}$ on the boundary of Ω is:

$$\underline{\nabla}\wedge\underline{v}=-\underline{\nabla}\wedge\begin{bmatrix}-\omega z_2\\ \omega z_1\\ 0\end{bmatrix}+\underline{\nabla}\wedge([\underline{\underline{Q}}^T]\cdot([\underline{V}]-[\underline{V}_{0'}]))=-\begin{bmatrix}0\\ 0\\ 2\omega\end{bmatrix} \tag{A7}$$

The velocity field $\underline{V}$, given by the macro-model, is the addition of the uniform stream that blows over the rotor and the field induced by the vortex net. All those fields are irrotational (the flow induced by a vortex filament is irrotational in every point except the singularity represented by the filament itself), so $\underline{V}$ is an irrotational field. Since $\underline{V}_{0'}$ is spatially constant, the second term of the second member of Eq. (A7) vanishes; and since ω is constant, $\underline{\nabla}\wedge\underline{v}$ is constant too.

We have proved that the curl of $\underline{v}$ is constant on the boundary of Ω; we have to prove now that it is so at every interior point. We shall apply the Kelvin's theorem of conservation of Γ to the integration of the velocity field along a closed material

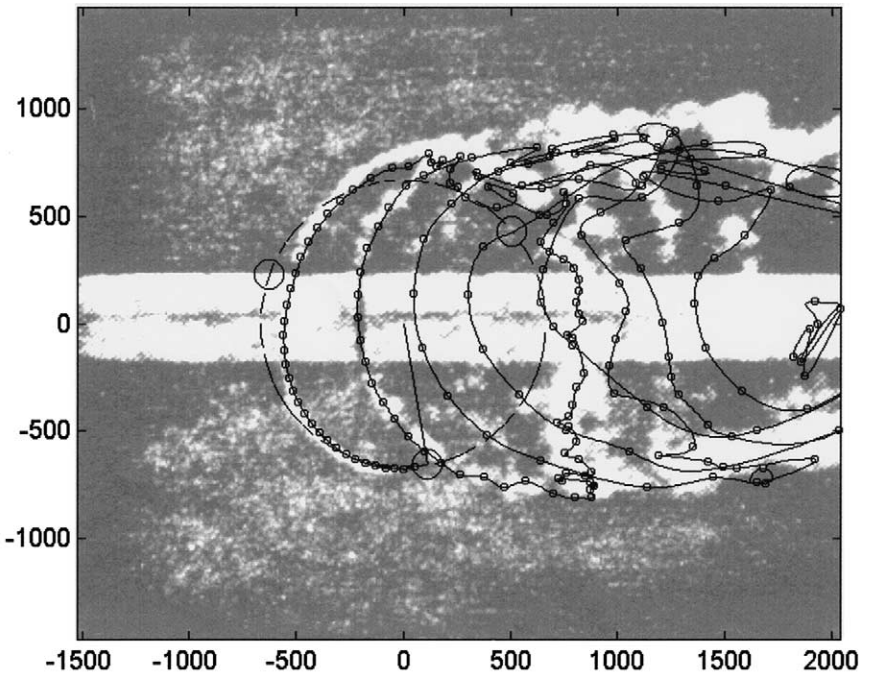

Fig. 12. Shed vortex centres path for a three-bladed rotor. Comparison of experimental visualisation [6] and FEVDTM prediction.

curve (a curve that touches the same particles at every time and follows their movement). Kelvin's theorem states that

$$\frac{d\Gamma_v}{dt}=0 \tag{A8}$$

Every material curve γ on the plane of analysis determines a material volume (an infinite tube with γ-shaped section). This tube displaces and deforms itself while following the particle's movement, but its volume could not change because of the incompressibility condition. The curve γ deforms itself too, but its enclosed area remains constant because of the bidimensional hypothesis.

Now, we shall apply the Stokes' theorem to γ:

$$\Gamma_v=\int_{\gamma}\underline{v}\cdot\hat{t}_\gamma d\gamma=\int_{S_\gamma}(\underline{\nabla}\wedge\underline{v})\cdot\hat{n}_\gamma ds \tag{A9}$$

where S_γ is the area enclosed by γ, $\hat{t}_\gamma$ is the unit vector tangent to γ and $\hat{n}_\gamma$ is the unit vector perpendicular to S_γ.

By Eq. (A8) Γ_v remains constant:

$$\int_{S_\gamma} (\underline{\nabla} \wedge \underline{v}) \cdot \hat{n}_\gamma ds = const. \tag{A10}$$

S_γ could be chosen arbitrarily. In particular, we can choose a tube with an infinitesimal cross section ΔS_γ, so we can consider a constant value for the curl over this infinitesimal area. Then, from Eq. (A10) we obtain:

$$(\underline{\nabla} \wedge \underline{v}) \Delta S_\gamma = const. \tag{A11}$$

As we state above, ΔS_γ must remains constant so:

$$(\underline{\nabla} \wedge \underline{V}) = const. \tag{A12}$$

The derivative in Eq. (A8) is a material derivative, so the result of Eq. (A12) implies that the curl of $\underline{v}$ must remain constant while it follows the particle along its trajectory across Ω. Finally, as every particle inside Ω must have passed across the Ω's boundary, and, as we have proved (see Eq. (A7)) that on that boundary $(\underline{\nabla} \wedge \underline{v})_{S_\Omega} = const. = -2\omega_k$, we conclude that the curl is constant at every point of Ω and Eq. (5) holds too.

References

[1] Templin RJ. Aerodynamic performance theory for the NRC vertical axis wind turbine. NCR of Canada TR, LTR–LA–160, 1974.
[2] Strickland JH. The Darrieus turbine: a performance prediction model using multiple streamtubes. Sandia Laboratory Report SAND 75–041, 1975.
[3] Paraschivoiu I. Aerodynamic loads and performance of the Darrieus rotor. AIAA J of Energy 1982;6(6):406–12.
[4] Fanucci JB, Walters RE. Innovative wind: the theoretical performances of a vertical axis wind turbine; proceedings of the vertical axis wind turbine technology workshop. Sandia Laboratory Report SAND 76–5586, III 1976;61–93.
[5] Milne-Thomson LM. Theoretical Hydrodynamics. Macmillan and Co, 1952.
[6] Strickland JH, Webster BT, Nguyen T. A vortex model of the Darrieus turbine: an analytical and experimental study. Trans ASME J Fluid Engng 1979;101:500–5.
[7] Wilson RE, Lissaman PBS, James M, McKie WR. Aerodynamic loads on a Darrieus rotor blade. Trans ASME J Fluid Engng 1983;105:53–8.
[8] Ponta FL. Análisis fluidodinámico de una hidroturbina de eje vertical. PhD thesis, School of Engineering, University of Buenos Aires, 1999.
[9] Klimas PC. Darrieus rotor aerodynamics. Trans ASME J Solar Energy Engng 1982;104:102–5.